Theor Chem Acc (2012) 131:1098
DOI 10.1007/s00214-012-1098-x

REGULAR ARTICLE

# $Mg^{2+}/Ca^{2+}$ binding to DNA bases: a quantum chemical method and ABEEM$\sigma\pi$/MM fluctuating charge model study

**Chun-Yang Yu · Yang Yu · Li-Dong Gong · Zhong-Zhi Yang**

Received: 6 August 2011 / Accepted: 3 November 2011 / Published online: 7 March 2012


**Abstract** The interactions of $Mg^{2+}$ and $Ca^{2+}$ binding to adenine, cytosine, guanine, and thymine at various binding sites were studied by a high-level quantum chemical method and ABEEM$\sigma\pi$/MM fluctuating charge model. The geometries and binding energies of $M^{2+}$-bases complexes were determined at CCSD(T)/6-311 ++G(2d,2p)//MP2/6-311 ++G(2d,2p) level of theory, with the basis set superposition error corrections for the binding energy calculations. In comparison with the ab initio results, an accurate classical metal cation–base interaction potential was constructed and parameterized in terms of ABEEM$\sigma\pi$/MM model. It is revealed that $Mg^{2+}/Ca^{2+}$ prefers to bind with bases at the bidentate position (between two nitrogen atoms or oxygen and nitrogen atoms in purine and pyrimidine), where the binding energy is the largest. Moreover, the distance between $M^{2+}$ and the base increases from $Mg^{2+}$ to $Ca^{2+}$, while the binding energy of $Mg^{2+}$–base is greater than that of $Ca^{2+}$-base. The ABEEM$\sigma\pi$/MM potential gives reasonable geometries and binding energies compared with the present quantum chemical calculations, and the overall percentage RMSDs are 1.4 and 1.6% for geometries and binding energies, respectively. Furthermore, the transferability of the parameters of the new potential is validated by investigation of $Mg^{2+}/Ca^{2+}$ binding to tautomer of bases, and results from our potential also show quite good consistency with those of MP2/6-311 ++G(2d,2p)//B3LYP/6-311 ++G(d,p) method, with the overall percentage RMSDs of 2.2 and 4.7% for geometries and binding energies, respectively. This work will serve as a basis for further investigations of the mechanisms of cation effects on the structure and property of nucleic acids.

**Keywords** DNA base · Metal cation · Quantum chemical method · ABEEM$\sigma\pi$/MM · Polarizable force field

## 1 Introduction

It is undisputable that metal ions play a crucial role in many biochemical processes that sustain life, and they are essential for several cell reactions and varied metabolic and physiological functions. Small deviations from normal levels of concentrations of some metal ions are recognized as symptoms of malfunctions or diseases [1–3]. These cations can modify electron flow in a substrate or enzyme, thus effectively controlling an enzyme-catalyzed reaction. The structure, stability, and function of DNA and RNA nucleic acids are also influenced by the presence of metal ions due to the negatively charged phosphate–sugar backbone [4–13]. Although the binding of metal ions to nucleic acids has been a subject of study for many years, the mechanisms of the cation effects on the structure and physical properties of DNA have not yet been clarified. The divalent cations can stabilize purine–purine–pyrimidine DNA triplexes [2], can favor the formation of rare tautomers and mispairs [5], can induce proton transfer between guanine N1 and cytosine N3 positions in Watson–Crick base pairs [6], and can interact favorably with $\pi$-systems causing the bases to unstuck [7]. The main effect of metal cations to DNA is to neutralize the negatively charged backbone phosphate–sugar groups through

**Electronic supplementary material** The online version of this article (doi:10.1007/s00214-012-1098-x) contains supplementary material, which is available to authorized users.

C.-Y. Yu · Y. Yu · L.-D. Gong (✉) · Z.-Z. Yang
School of Chemistry and Chemical Engineering, Liaoning Normal University, Dalian 116029, China
e-mail: gongjw@lnnu.edu.cn

non-specific electrostatic interactions. In addition, metal bindings may occur through a specific coordination of the metal ion either directly to the phosphate as well as (very rarely) to the sugar oxygen atoms and to the base nitrogen and oxygen sites (inner-sphere coordination) or via bridging water molecules (outer-sphere coordination), and the different coordinations depending on the concentration and on the kind of metal cation. For instance, metal ions that preferentially bind to nucleobases may cause more dramatic effects on DNA conformation than those binding to the phosphate and sugar backbone [8]. Therefore, although cation–phosphate interactions are predominant, the binding of metal ions to the bases is not negligible. One illustrative case is the cisplatin molecule, which links two consecutive bases together and is used as an anticarcinogenic drug [14, 15]. Many efforts have been devoted to investigate the fundamental nature of these interactions as well as to determine the cation affinity of nucleobases, both experimentally [16–24] and theoretically [25–48].

Recent advances in ab initio quantum chemistry and computer technology have greatly facilitated theoretical investigations of the interactions of metal ions with nucleobases. Despite the large computational cost of quantum chemistry methods (QM), they are the most useful approach in this field. Here, we will only introduce some of the many excellent works. Hobza and Šponer et al. presented systematic investigations on the interactions between the DNA bases, base pairs, and nucleotides with various mono- and divalent metal cations using quantum mechanical methods [28–32]. They found that intermolecular metal-$N_7$ distances for complexes containing adenine are shorter than those for complexes containing guanine, and the stabilization energies for guanine…metal complexes are larger than those of adenine…metal complexes. Recently, they studied the interactions of all tautomers of adenine, cytosine, thymine, and the eight most stable Keto/Enol tautomers of guanine with $Na^+$, $Mg^{2+}$ and $Zn^{2+}$ using a high-level ab initio method and found that the interaction of $Na^+$, $Mg^{2+}$, and $Zn^{2+}$ cations with cytosine in the gas phase will not induce a change from the canonical form to the rare tautomeric form. In the case of isolated guanine, the equilibrium of the canonical form with rare tautomers can be found. For isolated adenine and thymine, the presence of rare tautomers is highly probable. Russo and Toscano et al. employed density function theory (DFT) using the B3LYP hybrid potential to investigate $Li^+$, $Na^+$, $K^+$, $Mg^{2+}$, $Ca^{2+}$, $Al^{3+}$, and transition metal ions affinities to DNA and RNA bases in the gas phase. The effects of the size and charge of each cation on the organization of the surrounding water molecules were also analyzed [33–35]. The tautomerism in the most stable isomers of Al–guanine complexes and their cations, as well as the solvation of Al–guanine with an ammonia molecule, are researched with DFT and MP2 calculations by Vázquez and Martinez et al. More recently, they also studied the stabilization of different tautomers of cytosine Ca-, Zn-, and Cd-cytosine in neutral and ionic forms at the B3LYP/LANL2DZ level [38–40]. Sodupe and his colleagues studied the binding of first-row transition metal monocations ($Sc^+$-$Cu^+$) to N7 of guanine and N7 or N3 of adenine nucleobases, as well as the intermolecular proton-transfer processes in the Watson and Crick guanine–cytosine, adenine–thymine $Cu^+/Cu^{2+}/Ca^{2+}$ cationized base pairs by using the B3LYP method [41–43].

Moreover, classical molecular mechanics (MM) using predefined potentials are well established as a powerful tool serving to investigate biomolecular systems [49]. However, one of the major limitations with respect to the accuracy of the majority of MM force fields is the way in which the charge distribution of the molecules is treated. Typically, effective partial fixed charges are assigned to the atoms independent of the environment, and thus the created Coulomb interaction potentials are certainly not capable of adapting the charge distributions to changes of polarity in the environment, especially for cation-containing systems, where polarization and charge transfer are very important. In view of the significance of the polarization effect, much has been achieved since the 1970s in the development and employment of the polarizable force field (PFF) [50, 51] for biomolecular simulation. Three approaches are commonly used to treat the polarization effect, that is, the induced dipole model, the classical Drude oscillator model, and the fluctuating charge model. The induced dipole model consists of both partial atomic charges and inducible dipoles on the atoms comprising the molecular system [52–54]. In the classical Drude oscillator model, also known as the ''shell'' or ''charge on spring'' model, the polarizability is introduced via the inclusion of a single auxiliary charge (Drude) particle attached to each non-hydrogen atom by a harmonic spring. It is noteworthy that the CHARMM Drude PFF has been successfully developed for a wide range of systems encompassing water [56, 57], ions [58], and organic molecules [59–62], especially for the significant progress for nucleic acid bases by Baker and Anisimov et al. [63] most recently. The fluctuating charge models introduce polarizability into standard energy functions by allowing the values of the partial charges to respond to the electric field of their environment, thereby altering the molecular polarizability [64, 65]. This may be performed by coupling the charges to their environment using electronegativity equalization (EE) or chemical potential equalization (CPE) schemes. Simulations of ionic systems using non-polarizable additive force fields have shown that consideration of non-additive effects is important to accurately reproduce the atomic details of ions-related system [58]. The hybrid QM/MM [66–68] approach

is a nice tool to investigate ionic system. But, the choice of the size of the QM region is still something of an art. Meanwhile, although the QM region polarizes in response to the MM partial charges, the reverse is not also true (although fully polarizable QM/MM methods are being developed). Based on the atom-bond electronegativity equalization method (ABEEM) [69–71] fused into MM, Yang et al. [72–74] have established a new generation of polarization molecular force field, that is, the ABEEM$\sigma\pi$/MM fluctuating charge model. It has been applied successfully to the water system [72, 73], ion solvation [75–77], organic molecules [78], peptides [79], and nucleic acid [74, 75].

The present paper places emphasis on constructing an accurate fluctuating charge interaction potential between $Mg^{2+}$/$Ca^{2+}$ and DNA bases in terms of ABEEM$\sigma\pi$/MM model. The interactions between isolated bases and bare cations are the first step in explaining the effective role of metalation in the biophysics of nucleic acids. We selected the two metal ions because $Mg^{2+}$ and $Ca^{2+}$ are certainly the most abundant divalent cations within cells and because of their biological influence on the structure and property of DNA bases. Firstly, the ABEEM$\sigma\pi$/MM fluctuating charge potential is proposed and parameterized with reference to the binding energy from high-level ab initio results. Then the potential was applied to investigate the structures, binding energies, and charge distributions of the $Mg^{2+}$/$Ca^{2+}$–DNA base complexes. Finally, the reliability and transferability of the newly constructed potential were further validated by investigating $Mg^{2+}$/$Ca^{2+}$ binding to some tautomers of bases. The present work will serve as a basis for further investigations on the mechanisms of cation effects on the structure and property of nucleic acids, as well as other relevant important biological processes.

## 2 Theoretical model and computational methods

### 2.1 Quantum mechanical calculations

It is obvious that the nitrogen atom and oxygen atom of the DNA bases are the preferential sites for metal binding, and the bidentate position (between nitrogen atom and nitrogen/oxygen atom) is more favorable than the unidentate nitrogen/oxygen position indicated by QM calculations [32]. By a high-level QM calculation, we determined the favorable binding positions shown in Fig. 1. Adenine includes three favorable positions, two bidentate positions of (I) and (II) and one unidentate position (III); guanine includes three favorable bidentate positions (I)–(III); cytosine includes one bidentate position between O2 and N3; thymine includes two unidentate positions of O2 and O4, because of the repulsion between cation and the imino hydrogen (N3-H).

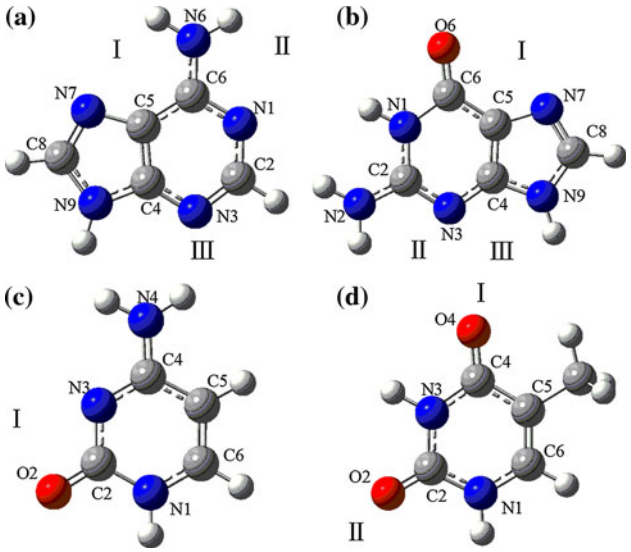


**Fig. 1** The possible coordination sites for metal cations in adenine (**a**), guanine (**b**), cytosine (**c**), and thymine (**d**)

The geometries and single-point energy of $M^{2+}$–base were determined at the CCSD(T)/6-311 ++G(2d,2p)//MP2/6-311 ++G(2d,2p) and MP2/6-311 ++G(2d,2p)//B3LYP/6-311 ++G(d,p) level of theory with the counterpoise correction for the basis set superposition error (BSSE) [80]. All the QM calculations were performed on an SGI Altix 3700 server by using the Gaussian 03 program package [81].

### 2.2 The ABEEM$\sigma\pi$/MM interaction potential and parameterization

To better account for the polarization effect in the ABEEM$\sigma\pi$/MM model, a molecular system is decomposed into regions of atoms, $\sigma$ and $\pi$ bonds, and lone-pairs, and each region is assigned by a partial charge. In Fig. 2, as an example, we present all charge sites of cytosine in ABEEM$\sigma\pi$ model. Better elucidation of the polarization effect from this partition scheme comes from the greater freedom and larger flexibility in calculating the fluctuating partial charge associated with each of the regions. In principle, if the total number of charge sites approaches infinity, the partial charge will resemble the continuous charge density, the fundamental variable of DFT. This is the essence and foundation of our ABEEM$\sigma\pi$ model. In addition, the cation–$\pi$ interactions have proven to be important in protein structures and biomolecule associations. Eric and his coworkers' calculations show that the major contribution to cation–$\pi$ interactions with DNA bases is of electrostatic nature [82]. Here, we just employ the Coulomb interaction between cation and $\pi$ charge sites in ABEEM$\sigma\pi$ base model.

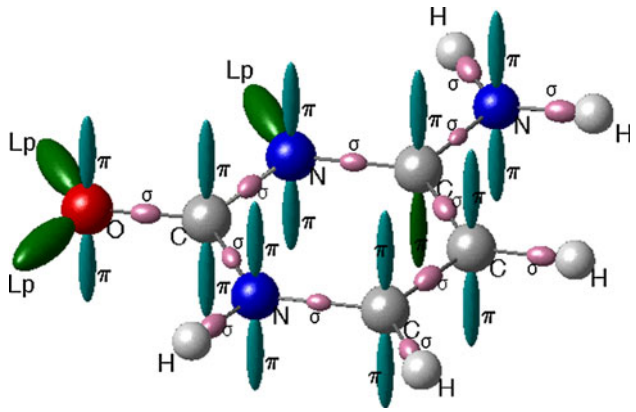


**Fig. 2** The sketch of ABEEM$\sigma\pi$ charge sites in cytosine

The potential function $E_{\mathrm{ABEEM/MM}}$ of $Mg^{2+}$/$Ca^{2+}$–bases system is expressed as

$$\begin{aligned} E_{\mathrm{ABEEM/MM}} &= \sum_{b=1}^{\text{bonds}} k_b(r_b - r_b^0)^2 + \sum_{a=1}^{\text{angles}} k_a(\theta_a - \theta_a^0)^2 \\ &+ \frac{1}{2}\sum_{t=1}^{\text{torsions}} [v_{t1}(1+\cos\varphi_t) + v_{t2}(1-\cos 2\varphi_t) \\ &+ v_{t3}(1+\cos 3\varphi_t)] \\ &+ \sum_{k=1}^{\text{imptors}} v_k(1-\cos 2j_k) \\ &+ \sum_{i<j}\left[4f_{ij}\varepsilon_{ij}\left(\frac{\sigma_{ij}^{12}}{R_{ij}^{12}} - \frac{\sigma_{ij}^{6}}{R_{ij}^{6}}\right) + k_{ij}\frac{q_i q_j e^2}{R_{ij}}\right] \end{aligned} \quad (1)$$

which stands for the bond stretching, the angle bending, dihedral angle torsion, improper torsion, van der Waals, and electrostatic interaction, respectively. $k_b$, $k_a$, $v_{t1}$, $v_{t2}$, $v_{t3}$, and $v_k$ represent the force constants of the bond stretching, angle bending, dihedral angle torsion, and improper torsion, respectively. $r_b^0$ and $\theta_a^0$ are used to denote the equilibrium values of the bond lengths and angles. $r_b$, $\theta_a$, and $\varphi_t$ stand for the real bond lengths, angles, and dihedral angles. Geometric combining rules for the Lennard–Jones coefficients are employed: $\sigma_{ij} = (\sigma_{ii}\sigma_{jj})^{1/2}$ and $\varepsilon_{ij} = (\varepsilon_{ii}\varepsilon_{jj})^{1/2}$. $R_{ij}$ is the distance between the site points $i$ and $j$. $f_{ij}$ is the coefficient of vdW interactions in the ABEEM/MM. If $i$ and $j$ are intramolecular, the coefficient $f_{ij} = 0.0$ for any $i - j$ pair connected by a valence bond (1–2 pairs) or a valence bond angle (1–3 pairs), $f_{ij} = 0.5$ for 1–4 interactions (atoms separated by three bonds), and $f_{ij} = 1.0$ for all other intramolecular and intermolecular cases. For the Coulomb term, $q_i$ and $q_j$ denote the site charges obtained from the ABEEM$\sigma\pi$ method (see Eq. 7 in Ref. [70]).

Parameters of the ABEEM/MM fluctuating charge model involves the ABEEM$\sigma\pi$ charge distribution parameters, that is, the valence-state electronegativity $\chi^*$, valence-state hardness $\eta^*$, and the force field parameters. Firstly, the ABEEM$\sigma\pi$ parameters of each charge site are obtained by fitting the QM Mulliken charge distribution through a regression and least-squares optimization procedure. The detailed formalisms and calibration of the parameters of ABEEM$\sigma\pi$ model can be found in Ref. [69–71]. In this study, the ABEEM$\sigma\pi$ parameters of the bases were taken from our previous work [74] without modification, and those for $Mg^{2+}$/$Ca^{2+}$ are listed in Table 1.

**Table 1** ABEEM and force filed parameters for $Mg^{2+}$ and $Ca^{2+}$

| Metal cation | $\chi^{*a}$ | $2\eta^{*b}$ | $\sigma$ | $\varepsilon$ |
|---|---|---|---|---|
| $Mg^{2+}$ | 1.5830 | 2.8530 | 2.1445 | 0.8750 |
| $Ca^{2+}$ | 1.2040 | 2.5850 | 2.4520 | 0.5497 |

[a] $\chi^*$ is the valence-state electronegativity

[b] $\eta^*$ is the valence-state hardness parameters

Then, we determined the force field parameters in Eq. 1, of which those for the bases were also taken from Ref. [74], including the bond stretching, angle bending, dihedral angle torsion, improper torsion, and vdW parameters. The parameters for the hard degrees of freedom (bond stretching and angle bending) were taken from AMBER. As for the "soft" degrees of freedom, the torsional and improper torsional parameters of AMBER were taken as a reference, and we refitted them through the least-squares optimization procedure to make the conformation energies and the key dihedral angles of the model molecules be in good agreement with those calculated by QM. In addition, the Lennard–Jones (LJ) parameters are determined by fitting QM conformational energies, base pair binding energies, dipole moments, and so on, using a regression and least-squares method.

The factor $k_{ij}$ is set to be 0.57 empirically in the ABEMM$\sigma\pi$ model [69–71] to correct electrostatic interactions between the charge sites, except for hydrogen bond regions. In order to effectively describe the hydrogen bond interaction, which is quite different from the common electrostatic interactions, we introduce a new parameter $k(R_{ij})$ in the hydrogen bond interaction region [72–74]. $k(R_{ij})$ is dependent on the distance of metal cation and lone-pair electron, $R_{ij}$, in the present study (Eq. 2). In terms of the Boltzmann function, we determined $k(R_{ij})$ by fitting the geometry and energy differences between QM and ABEEM$\sigma\pi$/MM at different distances near the equilibrium position between the metal cation and lone-pair for training set systems. The parameters of A, B, C, and D are listed in Table 2.

$$k(R_{ij}) = \mathrm{A} - \frac{\mathrm{B}}{1 + \exp[(R_{ij} - C)/D]} \quad (2)$$

In practice, $k(R_{ij})$ and LJ parameters of metal cations were conducted in concert to reproduce the QM geometries

**Table 2** Parameters in the function $k(R_{ij})_{base}$ for different metal cations, O/N pairs

| Type | A | B | C | D |
|---|---|---|---|---|
| Lp of N7 in A and $Mg^{2+}$ | 0.840 | 0.1306 | 1.1959 | 0.1197 |
| Lp of N6 in A/N9 in G and $Mg^{2+}$ | 0.727 | 0.1272 | 1.5664 | 0.0118 |
| Lp of N1, N3 in A/N3 in G and $Mg^{2+}$ | 0.776 | 0.1438 | 1.0108 | 0.0390 |
| Lp of N7 in G and $Mg^{2+}$ | 0.591 | 0.1420 | 1.1559 | 0.1369 |
| Lp of N2 in G and $Mg^{2+}$ | 0.600 | 0.1821 | 1.1989 | 0.1684 |
| Lp of N3 in C and $Mg^{2+}$ | 0.720 | 0.1337 | 1.2219 | 0.1177 |
| Lp of O4 in T and $Mg^{2+}$ | 0.650 | 0.1290 | 1.2375 | 0.1569 |
| Lp of O2 in C/O2 in T and $Mg^{2+}$ | 0.630 | 0.1205 | 1.1270 | 0.1287 |
| Lp of N7 in A and $Ca^{2+}$ | 0.735 | 0.1473 | 1.1256 | 0.1437 |
| Lp of N6 in A/N9 in G and $Ca^{2+}$ | 0.590 | 0.1517 | 1.2115 | 0.1602 |
| Lp of N1, N3 in A/N3 in G and $Ca^{2+}$ | 0.673 | 0.1031 | 1.2027 | 0.1107 |
| Lp of N7 in G and $Ca^{2+}$ | 0.615 | 0.1031 | 1.1244 | 0.1413 |
| Lp of N2 in G and $Ca^{2+}$ | 0.570 | 0.1917 | 1.2115 | 0.1037 |
| Lp of N3 in C and $Ca^{2+}$ | 0.760 | 0.1072 | 1.1943 | 0.1529 |
| Lp of O4 in T and $Ca^{2+}$ | 0.580 | 0.1985 | 1.5008 | 0.1857 |
| Lp of O2 in C/O2 in T and $Ca^{2+}$ | 0.560 | 0.1941 | 1.5180 | 0.1857 |

and binding energy of $Mg^{2+}$/$Ca^{2+}$–bases complexes, and additional manual iterative adjustment was involved.

## 3 Results and discussions

### 3.1 $Mg^{2+}$/$Ca^{2+}$–bases complexes

#### *3.1.1 Geometries*

Figure 3 depicts the graphical representation of different $M^{2+}$–base complexes studied in the present paper. As the most important structural parameters, the distances between $Mg^{2+}$/$Ca^{2+}$ and the N/O atom of the bases are listed in Fig. 3, in which the ABEEM$\sigma\pi$/MM results are shown firstly and the MP2/6-311 ++G(2d,2p) results are listed in parentheses. It is also meaningful to mention that our results, both the geometry and binding energy, from MP2/6-311 ++G(2d,2p)//B3LYP/6-311 ++G(d,p) are quite close to those from CCSD(T)/6-311 ++G(2d,2p)// MP2/6-311 ++G(2d,2p) calculations. The ABEEM$\sigma\pi$/MM geometries are in good agreement with those from the QM calculations, with small root mean square deviations (RMSDs) of 0.03 and 0.03 Å, and the maximum deviation of only 0.06 and 0.07 Å, relative to the MP2 and B3LYP results, respectively. The overall percentage RMSDs are 1.4% compared with the MP2 results.

As shown in Fig. 3, there are three cation-binding sites for adenine, and the complexes are denoted as a-$M^{2+}$-1, a-$M^{2+}$-2, and a-$M^{2+}$-3, respectively. In the case of a-$M^{2+}$-1, it favors the binding of $Mg^{2+}$/$Ca^{2+}$ in the bidentate position between the $N_6$ and $N_7$ atoms. The configuration of isolated adenine is planar, and the amino group is distorted when adenine interacts with the ion, which is due to the repulsion between the cation and hydrogen atoms in amino group. A similar situation occurs when $Mg^{2+}$ interacts with the $N_1$ and $N_6$ atoms in a-$Mg^{2+}$-2. However, the planar structure of amino group does not distorted in a-$Ca^{2+}$-2, which may be due to the much longer distance between the $N_6$ atom and $Ca^{2+}$. In a-$M^{2+}$-3, $Mg^{2+}$/$Ca^{2+}$ interacts with the $N_3$ atom solely, and the distance for $M^{2+}$-$N_3$ is reasonable to be shorter than those in a-$M^{2+}$-1 and a-$M^{2+}$-2.

In guanine there are also three sites to interact with $Mg^{2+}$/$Ca^{2+}$. The cation simultaneously interacts with the $O_6$ and $N_7$ atoms in g-$M^{2+}$-1, and the distance of $M^{2+}$-$O_6$ is shorter than that of $M^{2+}$-$N_7$, about 0.1 and 0.2 Å for $Mg^{2+}$ and $Ca^{2+}$, respectively. Moreover, g-$M^{2+}$-2 and g-$M^{2+}$-3 are fairly similar, and the amino and imino groups are distorted by the repulsion between the $N_2$-H or $N_9$-H hydrogen atom and the cation. Compared with g-$Mg^{2+}$-2, the distance of $Mg^{2+}$-$N_3$ in g-$Mg^{2+}$-3 extends by 0.02 Å (0.01Å by MP2 and 0.02 Å by B3LYP), while the distance of $Ca^{2+}$-$N_3$ in g-$Ca^{2+}$-3 contracts by 0.02 Å (0.01 Å by MP2 and 0.01 Å by B3LYP). But the distance of $M^{2+}$-$N_2$ in g-$M^{2+}$-2 is shorter than that of $M^{2+}$-$N_9$ in g-$M^{2+}$-3 by 0.07/0.08 Å for $Mg^{2+}$/$Ca^{2+}$ by ABEEM$\sigma\pi$/MM model (0.05/0.09 Å by MP2 method, 0.04/0.07 Å by B3LYP method), respectively.

In general, cytosine has fewer available binding positions than adenine and guanine. As shown in Fig. 3, only one stable structure denoted as c-$M^{2+}$ was found, in which the bidentate position $O_2\cdots M^{2+}\cdots N_3$ is available. Similarly as g-$M^{2+}$-1, the ABEEM$\sigma\pi$/MM distance of $M^{2+}$-$O_2$ (1.95/2.15 Å) is shorter than the corresponding distance of

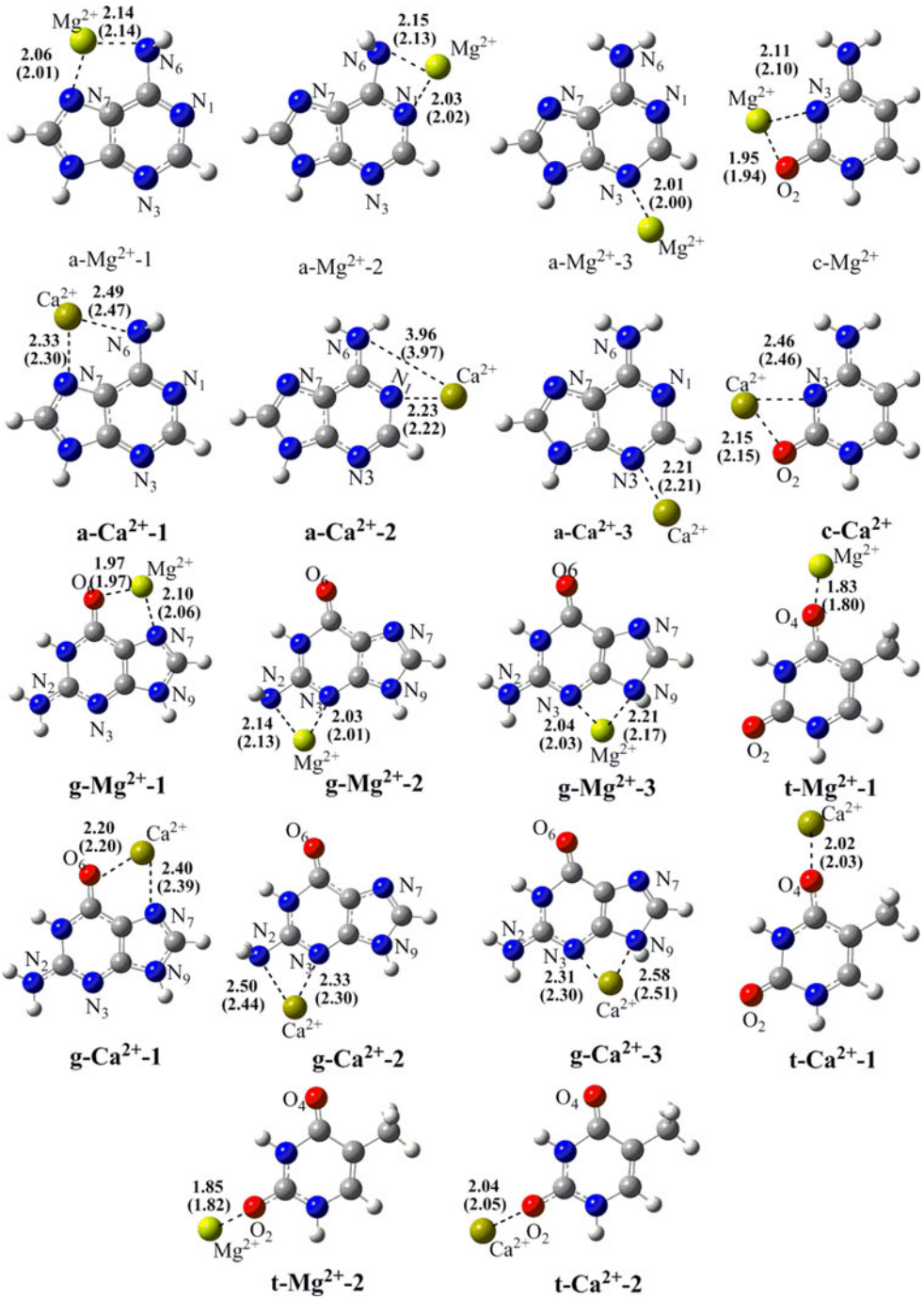


**Fig. 3** ABEEM$\sigma\pi$/MM-calculated structures of $Mg^{2+}$/$Ca^{2+}$–DNA base complexes, and the MP2/6-311 ++G(2d,2p) results (*in parentheses*) are also provided

$M^{2+}$-$N_3$ (2.11/2.46 Å) for $Mg^{2+}$ and $Ca^{2+}$, respectively, which is due to the attraction for the $O_2$ atom to $Mg^{2+}$/$Ca^{2+}$ is greater than that for the $N_3$ atom. Thymine has two carbonyl oxygen atoms, which provides two corresponding binding sites with cation, and the distance of $M^{2+}$-O changes inevidently from t-$M^{2+}$-1 to t-$M^{2+}$-2.

To summarize, three points should be mentioned: (1) When $Mg^{2+}$/$Ca^{2+}$ interacts with two nitrogen atoms, one of which belongs to an amino/imino group, the distance of $M^{2+}$-N is shorter than that of $M^{2+}$-$NH_2$ or $M^{2+}$-NH by at least 0.1 Å. This is mainly because of the repulsion between the cation and the H atoms of amino/imino group, which weakens the attraction between the nitrogen atom and $Mg^{2+}$/$Ca^{2+}$. (2) For guanine and cytosine, the distance of $M^{2+}$-O is shorter than that of $M^{2+}$-N by about 0.1 $\sim$ 0.2 Å for $Mg^{2+}$ and $Ca^{2+}$, respectively, owing to the fact that oxygen atom has stronger electronegativity than nitrogen. (3)As the ionic radius increases from $Mg^{2+}$ to $Ca^{2+}$, it is reasonable to find the increasing distance between $M^{2+}$ and the same base from $Mg^{2+}$ to $Ca^{2+}$.

**Table 3** Binding energies of $M^{2+}$–base complexes (kcal/mol)

| | ABEEM/MM | CCSD(T)[a] | MP2[b] | MP2[c] |
|---|---|---|---|---|
| a-$Mg^{2+}$-1 | 156.92 | 157.64 | 156.92 | 156.0 |
| a-$Mg^{2+}$-2 | 151.93 | 153.36 | 152.41 | 151.6 |
| a-$Mg^{2+}$-3 | 124.38 | 125.49 | 124.32 | 95.5 |
| a-$Ca^{2+}$-1 | 106.56 | 106.19 | 106.56 | |
| a-$Ca^{2+}$-2 | 87.00 | 84.12 | 85.35 | |
| a-$Ca^{2+}$-3 | 88.96 | 85.49 | 86.42 | |
| g-$Mg^{2+}$-1 | 190.04 | 191.05 | 190.05 | 189.0 |
| g-$Mg^{2+}$-2 | 133.75 | 132.95 | 133.75 | 132.4 |
| g-$Mg^{2+}$-3 | 119.15 | 120.03 | 116.78 | |
| g-$Ca^{2+}$-1 | 141.28 | 140.95 | 141.28 | |
| g-$Ca^{2+}$-2 | 91.15 | 85.69 | 87.35 | |
| g-$Ca^{2+}$-3 | 75.95 | 76.88 | 75.95 | |
| c-$Mg^{2+}$ | 175.63 | 176.55 | 175.63 | 173.9 |
| c-$Ca^{2+}$ | 130.67 | 130.42 | 130.68 | |
| t-$Mg^{2+}$-1 | 132.46 | 131.28 | 132.46 | 130.4 |
| t-$Mg^{2+}$-2 | 126.19 | 125.75 | 126.19 | 124.3 |
| t-$Ca^{2+}$-1 | 98.51 | 96.36 | 98.51 | |
| t-$Ca^{2+}$-2 | 93.48 | 91.82 | 93.48 | |
| RMSD[d] | | 1.93 | 1.28 | |

[a] CCSD(T)/6-311 ++G(2d,2p)//MP2/6-311 ++G(2d,2p) from this work

[b] MP2/6-311 ++G(2d,2p)//B3LYP/6-311 ++G(d,p) from this work

[c] MP2/TZVPP//MP2/TZVPP from Ref. [32]

[d] RMSD is of the ABEEM/MM binding energy in comparison with the CCSD(T) and MP2 results

### 3.1.2 Binding energies

The total binding energies, $\Delta E_{BE}$, of all the stable structures were calculated in terms of two QM methods mentioned above and ABEEM$\sigma\pi$/MM model, and the results are listed in Table 3. The binding energy is defined as:

$$\Delta E_{BE} = E_{M^{2+}} + E_{base} - E_{M^{2+}-base} \quad (3)$$

As can be seen from Table 3, ABEEM$\sigma\pi$/MM results are in excellent agreement with those of the QM calculations. Compared with the CCSD(T) and MP2 results, the RMSDs are only 1.93 and 1.28 kcal/mol, with the percentage RMSDs of 1.6 and 1.0%, and the linear correlation coefficient reaches 0.9989 (Fig. 4) and 0.9994, respectively.

For the adenine–$Mg^{2+}$ complexes, the most stable position is a-$Mg^{2+}$-1, and the binding energy is 156.92 kcal/mol by ABEEM$\sigma\pi$/MM. The binding energy in a-$Mg^{2+}$-2 is 151.93 kcal/mol, which is a little smaller than that of a-$Mg^{2+}$-1 and much greater than that of a-$Mg^{2+}$-3 by about 30 kcal/mol. However, the binding energy of a-$Ca^{2+}$-1 is larger than those of a-$Ca^{2+}$-2 and a-$Ca^{2+}$-3 about 20 kcal/mol, and the $\Delta E_{BE}$ of a-$Ca^{2+}$-2 is approximately equal to that of a-$Ca^{2+}$-3; the deviation between them is only 1.96 kcal/mol by ABEEM$\sigma\pi$/MM.

In the case of guanine–$Mg^{2+}$ complexes, g-$Mg^{2+}$-1 is the most stable one, and its binding energy reaches 190.04 kcal/mol. The binding energies for g-$Mg^{2+}$-2 and g-$Mg^{2+}$-3 are 133.75 and 119.15 kcal/mol, respectively. Although the guanine–$Ca^{2+}$ complexes are similar to guanine–$Mg^{2+}$ complexes, the corresponding binding energies decrease from 42.60 to 48.76 kcal/mol by ABEEM$\sigma\pi$/MM (43.15–50.10 kcal/mol by CCSD(T) method, and 40.83–48.77 kcal/mol by MP2 method).

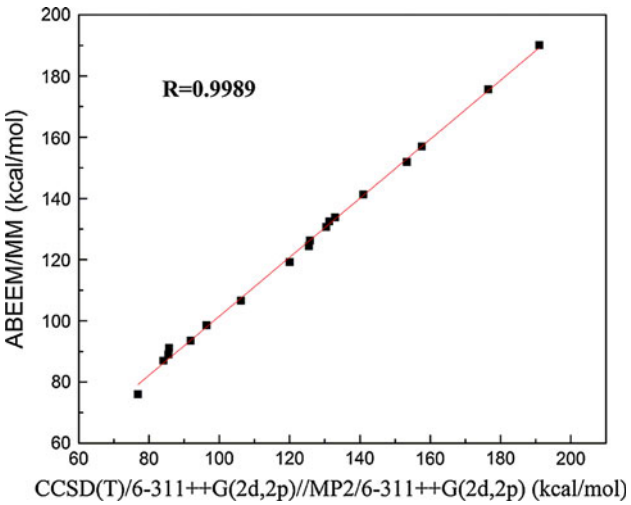


**Fig. 4** The ABEEM$\sigma\pi$/MM binding energies versus the corresponding CCSD(T) results of $Mg^{2+}$/$Ca^{2+}$–DNA base complexes

For the thymine–$M^{2+}$ complexes, $Mg^{2+}$/$Ca^{2+}$ interacts with two oxygen atoms of the bases, respectively. Complex t-$M^{2+}$-1 is relatively more stable than that of t-$M^{2+}$-2, and the binding energy of t-$M^{2+}$-1 is greater than that of t-$M^{2+}$-2 by 6.27 kcal/mol for $Mg^{2+}$ and by 5.03 kcal/mol for $Ca^{2+}$. The binding energy of cytosine–$M^{2+}$ complexes is greater than that of the same position of thymine–$M^{2+}$

complexes, because N3 atom in cytosine replaces N–H bond in thymine at the same site, so there is much more electrostatic attraction to metal cations. The binding energies of cytosine-$M^{2+}$ complexes by ABEEM$\sigma\pi$/MM are 175.63 and 130.67 kcal/mol for $Mg^{2+}$ and $Ca^{2+}$, respectively.

To sum up, the following order of relative binding ability of different sites with the metal cation in the DNA bases holds: $N_7$ (guanine) > $N_3$ (cytosine) > $N_7$ (adenine), and the other sites are uncertainty. Moreover, because the radius of $Mg^{2+}$ is smaller than that of $Ca^{2+}$, it is reasonable to find the binding energies of $Mg^{2+}$–base complexes are larger than those of corresponding $Ca^{2+}$–base complexes. The whole stabilization order of $M^{2+}$–base complexes are g-$Mg^{2+}$-1 > c-$Mg^{2+}$> a-$Mg^{2+}$-1 > a-$Mg^{2+}$-2 > g-$Mg^{2+}$-2 > t-$Mg^{2+}$-1 > t-$Mg^{2+}$-2 > a-$Mg^{2+}$-3 > g-$Mg^{2+}$-3 for $Mg^{2+}$, and g-$Ca^{2+}$-1 > c-$Ca^{2+}$> a-$Ca^{2+}$-1 > t-$Ca^{2+}$-1 > t-$Ca^{2+}$-2 > g-$Ca^{2+}$-2 > a-$Ca^{2+}$-3 > a-$Ca^{2+}$-2 > g-$Ca^{2+}$-3 for $Ca^{2+}$–base complexes.

As shown above, the ABEEM$\sigma\pi$/MM results are consistent with those from the two present quantum chemistry calculations.

### 3.1.3 ABEEM charge distribution

The ABEEM$\sigma\pi$ model computes the explicit charges of atoms, bonds, and lone-pair electrons, which are fluctuating with the different ambient environment. Moreover, we have specially treated the pairwise electrostatic interaction between metal ion and the lone-pair electron of atoms nitrogen and oxygen of bases, and given the specific expression of the interaction parameter $k(R_{ij})$ function in Eq. 2. In addition, the ABEEM/MM not only contain the fluctuating charge but also use the non-rigid-body molecule permitting vibration of bond length and angle of the bases. The ABEEM charge distributions of selected sites of the $M^{2+}$–bases complexes are presented in Table 4, from which we can see that the presence of $Mg^{2+}$/$Ca^{2+}$ near bases has strongly affected the charge distributions in the bases. The charges of both cations and bases are different compared with the isolated bases in all the selected sites and cations, which is consequential upon the interactions between cation and base. The significant changes take place in the cation, and the lone-pair directly interacts with the cation. For example, for complex a-$Mg^{2+}$-1, obvious polarization and charge transfer can be seen from the charge variations of the sites $lpN_7$, $lpN_6$, and $Mg^{2+}$, which are −0.49, −0.25, and −0.42, respectively. We can also find that the charge transfer from cation to base is generally larger for $Mg^{2+}$–base complex than that for the corresponding $Ca^{2+}$–base complex. For example, the charge transfer of $M^{2+}$ in a-$M^{2+}$-1 is 0.42 and 0.39 for $Mg^{2+}$ and $Ca^{2+}$, respectively, which is also because of the smaller radius of $Mg^{2+}$. It is also meaningful to notice the greater charge transfer for $Ca^{2+}$ (0.61) than $Mg^{2+}$ (0.53) in a-$M^{2+}$-2 complexes. This is due to the distorted amino group in a-$Mg^{2+}$-2 (Fig. 3), which further manifests that our model can represent responses as the structure of the system changes. To summarize, the fluctuating charge ABEEM$\sigma\pi$/MM model can reasonably reflect the changed ambient environment or structure and make a compensation for the shortage of fixed-point charge models.

## 3.2 $Mg^{2+}$/$Ca^{2+}$–tautomeric base complexes

In this section, we will validate the transferability of the parameters and examine the newly constructed ABEEM$\sigma\pi$/MM potential by comparing the optimized geometries and binding energies of $Mg^{2+}$/$Ca^{2+}$–tautomeric bases from ABEEM$\sigma\pi$/MM and the ab initio results. As has been shown above, the MP2/6-311 ++G(2d,2p)//B3LYP/6-311 ++G(d,p) method can give results as accurately as CCSD(T)/6-311 ++G(2d,2p)//MP2/6-311 ++G(2d,2p) method does for $Mg^{2+}$/$Ca^{2+}$–bases complexes. Hence, the MP2/6-311 ++G(2d,2p)//B3LYP/6-311 ++G(d,p) level of theory was employed for the computational efficiency to study complexes of $Mg^{2+}$/$Ca^{2+}$ with tautomeric bases. Here, we selected 14 typical tautomers of bases for the present study.

### 3.2.1 Geometries

Figures 5 and 6 depict the graphical representation of $M^{2+}$–tautomers of bases complexes in the present study. We can see that the ABEEM$\sigma\pi$/MM potential gives reasonable geometries compared with those of the B3LYP calculations, and the RMSD is only 0.06 Å, which equates a percentage RMSD of 2.2%.

As shown in Fig. 5, the amino group is distorted when tautomers a1 and a2 interact with $Mg^{2+}$, which is the same as $Mg^{2+}$ interacted with canonical adenine. However, a1ca and a2ca have the opposite situations owing to the longer distances between $Ca^{2+}$ and N atom, and the ABEEM$\sigma\pi$/MM model and B3LYP method give the same value of 4.63 and 3.97 Å, respectively. The metal cations interacted with imino N atom in a3 $M^{2+}$1 and a3 $M^{2+}$2 complexes directly. And the distances of $Mg^{2+}$-N in both are 1.96 Å by ABEEM$\sigma\pi$/MM (1.95 and 2.01 Å by B3LYP, respectively). Meanwhile, the distances of $Ca^{2+}$-N are 2.18 and 2.30 Å by ABEEM$\sigma\pi$/MM (2.16 and 2.30 Å by B3LYP method), respectively. The difference between a3 and a4 is the directions of the imino H atom. However, the structure of complex a3 $M^{2+}$2 is very similar to a4 $M^{2+}$1 because of repulsion between metal cations and hydrogen atom. Complexes a3 $M^{2+}$3 are similar to a-$M^{2+}$-3, in which $M^{2+}$ binds to N3 atom, and the distances of $M^{2+}$-N are 2.06 and 2.01 Å for $Mg^{2+}$, and 2.27 and 2.21 Å for $Ca^{2+}$ by ABEEM$\sigma\pi$/MM potential, respectively.

**Table 4** ABEEM charge distributions of selected sites for $M^{2+}$–bases complexes

| | $lpN_1$ | $lpN_3$ | $lpN_7$ | $lpN_6$ | | | $Mg^{2+}/Ca^{2+}$ |
|---|---|---|---|---|---|---|---|
| Adenine | −0.18 | −0.17 | −0.18 | −0.10 | | | |
| a-Mg-1 | −0.22 | −0.21 | −0.67 | −0.35 | | | 1.58 |
| a-Mg-2 | −0.62 | −0.21 | −0.22 | −0.33 | | | 1.48 |
| a-Mg-3 | −0.23 | −0.63 | −0.22 | – | | | 1.42 |
| a-Ca-1 | −0.23 | −0.22 | −0.55 | −0.29 | | | 1.61 |
| a-Ca-2 | −0.50 | −0.23 | −0.23 | – | | | 1.39 |
| a-Ca-3 | −0.24 | −0.50 | −0.23 | – | | | 1.40 |
| | $lpN_7$ | $lpO_6$ | $lpO_6$ | $lpN_3$ | $lpN_2$ | $lpN_9$ | |
| Guanine | −0.32 | −0.21 | −0.23 | −0.19 | −0.14 | −0.09 | |
| g-Mg-1 | −0.83 | −0.66 | −0.30 | −0.22 | – | – | 1.62 |
| g-Mg-2 | −0.38 | −0.25 | −0.27 | −0.60 | −0.28 | – | 1.41 |
| g-Mg-3 | −0.38 | −0.25 | −0.27 | −0.53 | – | −0.35 | 1.37 |
| g-Ca-1 | −0.84 | −0.45 | −0.34 | −0.23 | – | – | 1.67 |
| g-Ca-2 | −0.39 | −0.26 | −0.28 | −0.48 | −0.25 | – | 1.49 |
| g-Ca-3 | −0.39 | −0.26 | −0.28 | −0.42 | – | −0.24 | 1.41 |
| | $lpN_3$ | $lpO_2$ | $lpO_2$ | | | | |
| Cytosine | −0.17 | −0.20 | −0.18 | | | | |
| c-Mg | −0.50 | −0.28 | −0.62 | | | | 1.53 |
| c-Ca | −0.50 | −0.32 | −0.45 | | | | 1.60 |
| | $lpO_4$ | $lpO_4$ | $lpO_2$ | $lpO_2$ | | | |
| Thymine | −0.20 | −0.20 | −0.20 | −0.20 | | | |
| t-Mg-1 | −0.58 | −0.48 | −0.25 | −0.26 | | | 1.51 |
| t-Mg-2 | −0.25 | −0.26 | −0.49 | −0.53 | | | 1.35 |
| t-Ca-1 | −0.46 | −0.45 | −0.27 | −0.27 | | | 1.49 |
| t-Ca-2 | −0.27 | −0.28 | −0.43 | −0.44 | | | 1.45 |

For tautomeric guanine, there still exists bidentate position in complexes g1 $M^{2+}$1 and g2 $M^{2+}$. In g1 $M^{2+}$1, $M^{2+}$ binds with two N atoms, while in g1 $M^{2+}$2, $M^{2+}$ binds with the carbonyl O atom. For g2 $M^{2+}$, $M^{2+}$ binds with N and O atoms, in which the distance of $M^{2+}$–O is shorter than that of $M^{2+}$–N by about 0.15–0.30 Å. For the cytosine tautomers, only one metalated structure can be found, and it corresponds to the metal binding with O2 and N3. The distances between the cation and tautomeric cytosine in c1 $M^{2+}$ and c2 $M^{2+}$ have tiny differences due to different positions of imino H atoms. Similar situation can also be seen for the tautomeric thymine,that is, t1 $M^{2+}$ and t2 $M^{2+}$.

### 3.2.2 Binding energies

Table 5 lists the binding energies of the $M^{2+}$–tautomer of base complexes from the ABEEM$\sigma\pi$/MM potential and the MP2 methods, from which we can see that the ABEEM$\sigma\pi$/MM binding energies are in fair agreement with those from MP2 method, and the RMSD is 6.29 kcal/mol, equating to a percentage RMSD of 4.7%, with a linear correlation coefficient of 0.9886 (Fig. 7).

It should be mentioned that the binding energy of the most energy-favored structure of the metalated tautomer, that is, a4mg1, exceeds the canonical form, a-$Mg^{2+}$-1, by as much as 36 kcal/mol, calculated from ABEEM$\sigma\pi$/MM (41 kcal/mol by MP2 method). This shows that binding of metal cation to the bidentate position will dramatically change the relative stabilities of various tautomers and even cause the preference of unusual tautomer to be more pronounced. The binding energies of g2 mg/g2ca are greater than those of g-Mg-1/g-Ca-1 by 13.78/11.04 kcal/mol from ABEEM/MM calculations (15.52/14.26 kcal/mol by MP2 method), respectively. It should be mentioned that the energy differences between these structures are mainly due to the different position of hydrogen atom. The other reason is because the cation binds to the base at a bidentate position of N and O, which is more energy-favored.

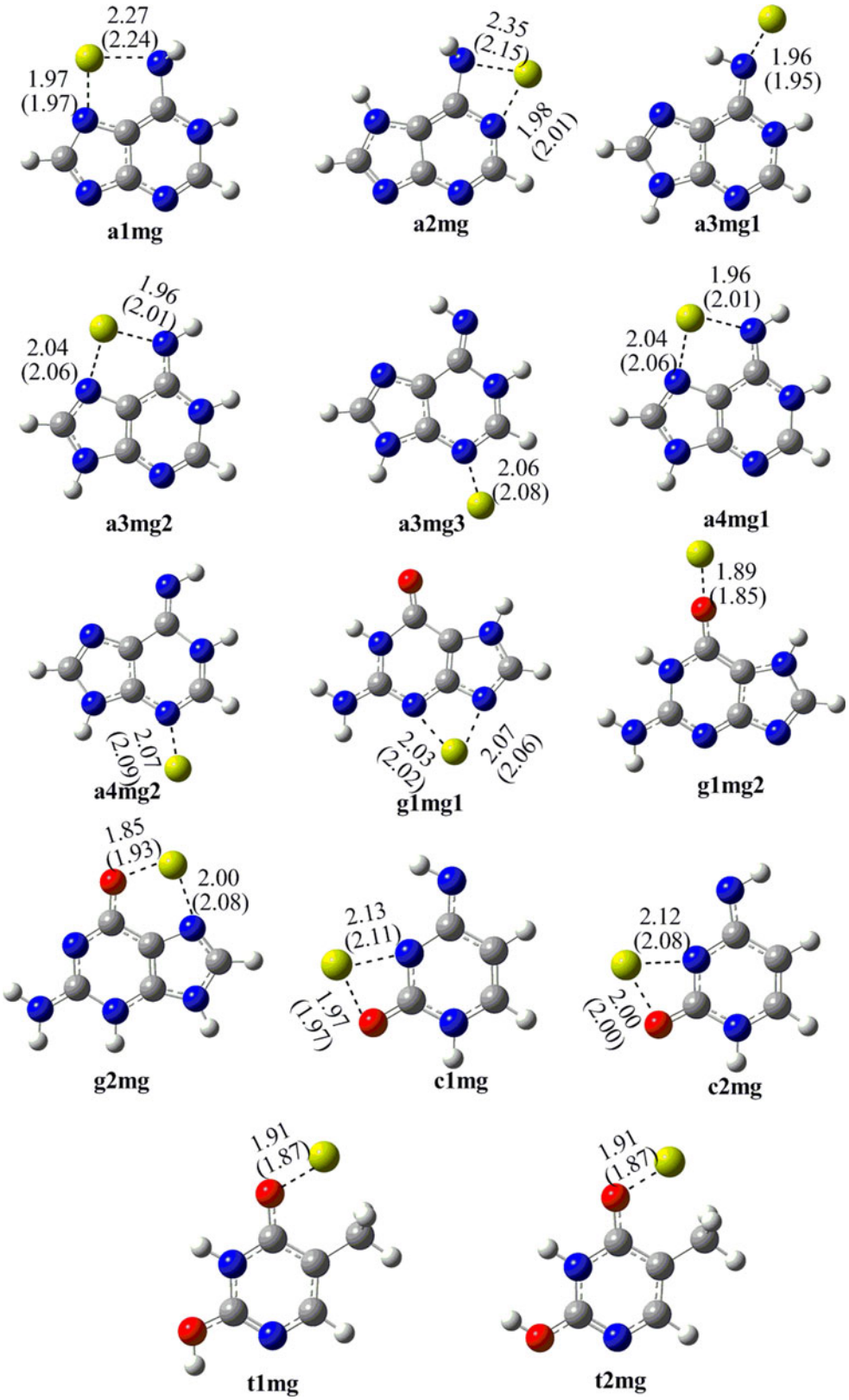


**Fig. 5** The ABEEM$\sigma\pi$/MM-calculated structures of $Mg^{2+}$–tautomer of DNA base complexes, and the B3LYP/6-311 ++G(d,p) results (*in parentheses*) are also provided

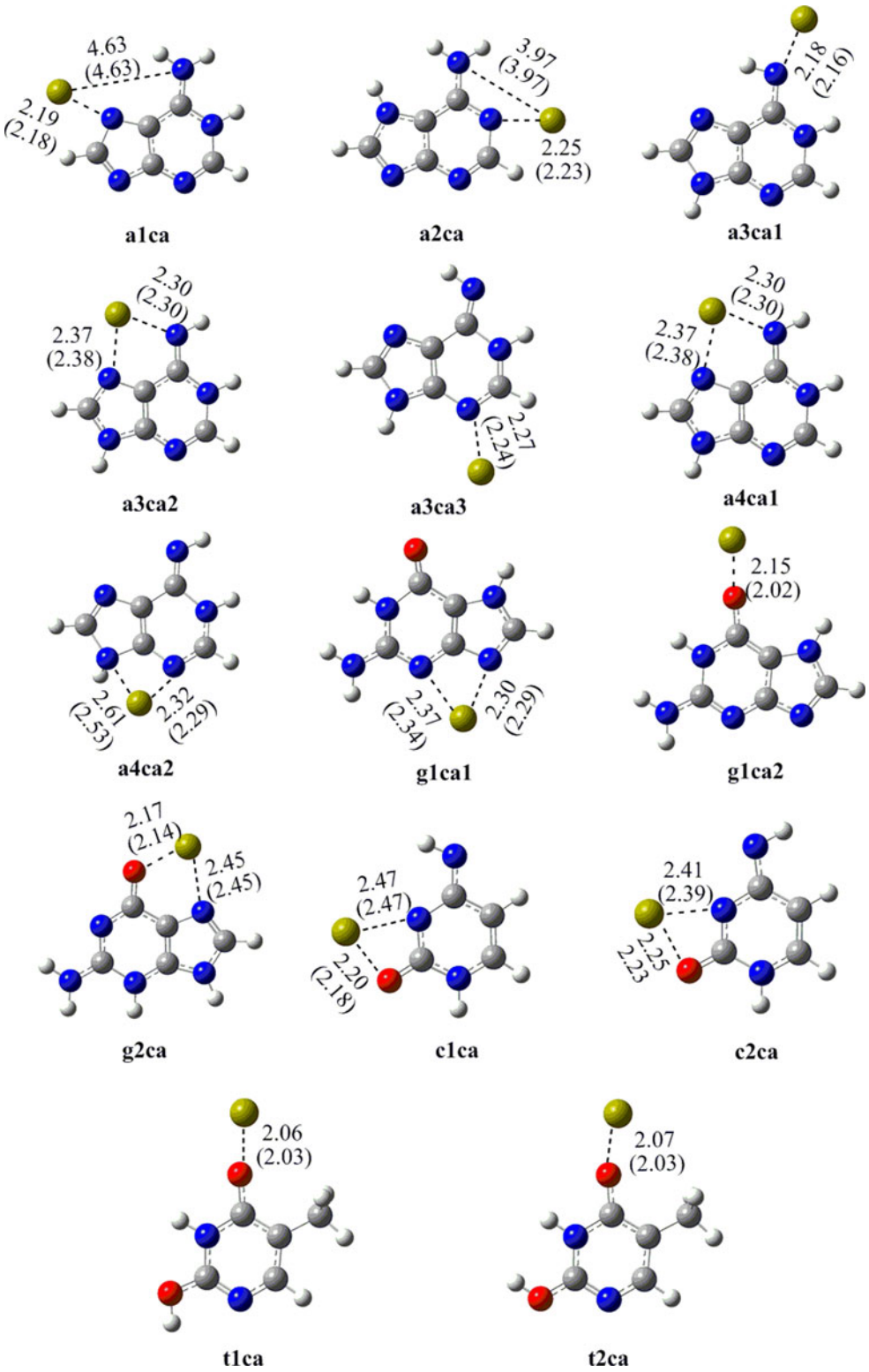


**Fig. 6** The ABEEM$\sigma\pi$/MM-calculated structures of $Ca^{2+}$–tautomer of DNA base complexes, and the B3LYP/6-311 ++G(d,p) results (*in parentheses*) are also provided

## 4 Conclusions

We have systematically investigated the interaction of $Mg^{2+}$/$Ca^{2+}$ with canonical DNA bases by high-level quantum mechanical method, and then we constructed an accurate interaction for the above system in the spirit of ABEEM$\sigma\pi$/MM fluctuating charge model. The parameters were determined in comparison with the quantum mechanical results. Results show that: (1) When $Mg^{2+}$/$Ca^{2+}$ interact with O and N atom of the bases

**Table 5** The binding energy of $M^{2+}$–tautomer of base complexes (kcal/mol)

| Type | ABEEM/MM | MP2[a] | Type | ABEEM/MM | MP2[a] |
|---|---|---|---|---|---|
| a1mg | 157.01 | 153.73 | a1ca | 102.87 | 95.43 |
| a2mg | 146.03 | 146.58 | a2ca | 64.61 | 82.63 |
| a3mg1 | 126.75 | 144.37 | a3ca1 | 94.89 | 103.03 |
| a3mg2 | 192.84 | 191.54 | a3ca2 | 136.34 | 138.62 |
| a3mg3 | 107.08 | 107.52 | a3ca3 | 71.60 | 68.73 |
| a4mg1 | 193.59 | 198.01 | a4ca1 | 137.02 | 145.08 |
| a4mg2 | 107.55 | 106.91 | a4ca2 | 71.93 | 74.51 |
| g1mg1 | 167.26 | 171.30 | g1ca1 | 123.36 | 125.22 |
| g1mg2 | 124.91 | 132.63 | g1ca2 | 94.46 | 99.24 |
| g2mg | 202.78 | 205.57 | g2ca | 152.32 | 155.54 |
| c1mg | 162.03 | 163.80 | c1ca | 120.67 | 121.87 |
| c2mg | 169.04 | 177.19 | c2ca | 135.46 | 135.31 |
| t1mg | 135.26 | 139.27 | t1ca | 97.67 | 101.97 |
| t2mg | 134.74 | 137.53 | t2ca | 98.33 | 99.08 |
| RMSD[b] | 6.10 | | | 6.48 | |

[a] MP2/6-311 ++G(2d,2p)// B3LYP/6-311G(d,p) from this work

[b] RMSD is of the ABEEM/MM binding energy in comparison with the MP2 results

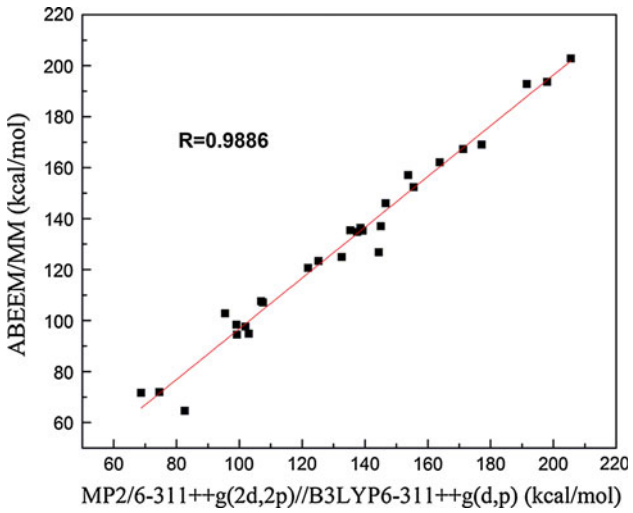


**Fig. 7** The ABEEM$\sigma\pi$/MM binding energies versus the corresponding MP2 results of $Mg^{2+}$/$Ca^{2+}$–tautomer of DNA base complexes

simultaneously, the distance of $M^{2+}$–O is shorter than that of $M^{2+}$–N. (2) The distance of $M^{2+}$–N is shorter than that of $M^{2+}$–$NH_2$ and that of $M^{2+}$–NH. (3) From $Mg^{2+}$ to $Ca^{2+}$, the distance from $M^{2+}$ to the same base increases with the increasing radius, while the binding energies decreases. (4) The binding energy order for DNA bases is: g-$Mg^{2+}$-1 > c-$Mg^{2+}$> a-$Mg^{2+}$-1 > a-$Mg^{2+}$-2 > g-$Mg^{2+}$-2 > t-$Mg^{2+}$-1 > t-$Mg^{2+}$-2 > a-$Mg^{2+}$-3 > g-$Mg^{2+}$-3 for $Mg^{2+}$, and g-$Ca^{2+}$-1 > c-$Ca^{2+}$> a-$Ca^{2+}$-1 > t-$Ca^{2+}$-1 > t-$Ca^{2+}$-2 > g-$Ca^{2+}$-2 > a-$Ca^{2+}$-3 > a-$Ca^{2+}$-2 > g-$Ca^{2+}$-3 for $Ca^{2+}$. For both $Mg^{2+}$ and $Ca^{2+}$, the order of preferred binding sites in different bases is $N_7$ (guanine) > $N_3$ (cytosine) > $N_7$ (adenine).

The ABEEM$\sigma\pi$/MM results are in good agreement with those of QM results, with a small root square deviation (RMSD) of 0.03 Å, equating to a percentage RMSD of 1.4%. For the binding energies, compared with the CCSD(T) and MP2 results, the RMSD of ABEEM$\sigma\pi$/MM is only 1.93 and 1.28 kcal/mol, equating to percentage RMSDs of 1.6 and 1.0%, and the linear correlation coefficient reaches 0.9989 and 0.9994, respectively. Furthermore, the transferability of the parameters of the new potential is validated by investigation of $Mg^{2+}$/$Ca^{2+}$ binding to tautomers of bases, and results from our potential also show quite good consistency with those of MP2/6-311 ++G(2d,2p)//B3LYP/6-311 ++G(d,p) method, with the overall percentage RMSDs of 2.2 and 4.7% for geometries and binding energies, respectively.

To sum up, the newly constructed ABEEM$\sigma\pi$/MM potential can accurately reproduce the ab initio structures and binding energies of $Mg^{2+}$/$Ca^{2+}$–base complexes. The presented potential will be applied and generalized to study hydrated metal cation binding to bases, base pairs, nucleotides, and dynamic simulations on the cation containing nucleic acid systems in the aqueous solution. Up to now, we have developed the ABEEM$\sigma\pi$/MM parameters for the bases, sugar ring, and phosphate group. The parameterizations for the interactions of metal cations and water, cation and phosphate, cation and sugar, etc. are still in process, and they will be conducted in concert to achieve a balanced description of all the interactions. In addition, as Baker et al. [63] pointed out most recently, to complete the development of a reliable force field for simulations of nucleic acids, the optimization of bond, angle, and dihedral parameters associated with different moieties in the combining process of these parameters, as well as the validation of the final models against condensed-phase data for

the full oligonucleotides, are still significant tasks. Shedding light on the mechanisms of metal ions effects on the structure and property of nucleic acids will be pursued in our future projects.

**Acknowledgments** The authors greatly thank Professor Jay William Ponder for providing the Tinker programs, and they are also grateful to the reviewers' helpful suggestions. This work was supported by the grants from the National Natural Science Foundation of China (Nos. 20703022, 21133005 and 21011120087) and the Education Bureau of Liaoning Province (No. 2009T057).

## References

1. Shier D, Buttler J, Lewis R (1996) Hole's human anatomy and physiology, 8th edn. McGraw-Hill, Boston
2. Bernues J, Azorin F (1995) In: Eckstein F, Lilley DMJ (eds) Nucleic acids and molecular biology. Springer, Berlin
3. Dupureur CM (2008) Curr Opin Chem Biol 12:250–255
4. Martin RB (1985) Acc Chem Res 18:32–38
5. Sigel H (1993) Chem Soc Rev 22:255–267
6. Gorb L, Podolyan Y, Dziekonski P, Sokalski WA, Leszczynski J (2004) J Am Chem Soc 126:10119–10129
7. Rodgers MT, Armentrout PB (2002) J Am Chem Soc 124:2678–2691
8. Shin YA, Eichhorn GL (1977) Biopolymers 16:225–230
9. Chiu TK, Dickerson RE (2000) J Mol Biol 301:915–945
10. Egli M (2002) Chem Biol 9:277–286
11. Noguera M, Ríos-Font R, Rodríguez-Santiago L, Solans-Monfort X, Oliva A, Bertran J, Sodupe M (2009) Theor Chem Acc 123:105–111
12. Muller J (2010) Metallomics 2:318–327
13. Fan HY, Shek YL, Amiri A, Dubins DN, Heerklotz H, Macgregor RB, Chalikian TV (2011) J Am Chem Soc 133:4518–4526
14. Rosenberg B, Vancamp L, Trosko JE, Mansour VH (1969) Nature 222:385–386
15. Melchior A, Sánchez Marcos E, Pappalardo RR, Martínez J (2011) Theor Chem Acc 128:627–638
16. Rodgers MT, Armentrout PB (2000) J Am Chem Soc 122:8548–8558
17. Sigel H, Kapinos LE (2000) Coor Chem Rev 200–202:563–594
18. Anastassopoulou J (2003) J Mol Struct 651–653:19–26
19. Freisinger E, Sigel RKO (2007) Coor Chem Rev 251:1834–1851
20. Wang P, Polce MJ, Ohanessian G, Wesdemiotis C (2008) J Mass Spectrom 43:485–494
21. Gillis EAL, Rajabi K, Fridgen TD (2009) J Phys Chem A 113:824–832
22. Krasnokutski SA, Lee JS, Yang D-S (2010) J Chem Phys 132:044304
23. Rajabi K, Gillis EAL, Fridgen TD (2010) J Phys Chem A 114:3449–3456
24. Sigel RKO, Sigel H (2010) Acc Chem Res 43:974–984
25. Perahia D, Pullman A, Pullman B (1977) Theor Chem Acc 43:207–214
26. Pullman A, Ebbesen T, Rholam M (1979) Theor Chem Acc 51:247–254
27. Cauchy D, Lavery R, Pullman B (1980) Theor Chem Acc 57:323–327
28. Burda JV, Sponer J, Hobza P (1996) J Phys Chem 100:7250–7255
29. Šponer J, Sabat M, Gorb L, Leszczynski J, Lippert B, Hobza P (2000) J Phys Chem B 104:7535–7544
30. Muñoz J, Sponer J, Hobza P, Orozco M, Luque FJ (2001) J Phys Chem B 105:6051–6060
31. Sychrovsky V, Sponer J, Hobza P (2004) J Am Chem Soc 126:663–672
32. Kabeláč M, Hobza P (2006) J Phys Chem B 110:14515–14523
33. Russo N, Toscano M, Grand A (2001) J Am Chem Soc 123:10272–10279
34. Russo N, Toscano M, Grand A (2001) J Phys Chem B 105:4735–4741
35. Russo N, Toscano M, Grand A (2003) J Phys Chem A 107:11533–11538
36. Gu J, Leszczynski J (2001) J Phys Chem A 106:529–532
37. Gu J, Leszczynski J (2001) J Phys Chem A 105:10366–10371
38. Moussatova A, Vázquez M-V, Martínez A, Dolgounitcheva O, Zakrzewski VG, Ortiz JV, Pedersen DB, Simard B (2003) J Phys Chem A 107:9415–9421
39. Vázquez M-V, Moussatova A, Martínez A, Dolgounitcheva O, Zakrzewski VG, Ortiz JV (2004) J Phys Chem A 108:5845–5850
40. Vázquez M-V, Martínez A (2007) J Phys Chem A 111:9931–9939
41. Noguera M, Bertran J, Sodupe M (2004) J Phys Chem A 108:333–341
42. Noguera M, Branchadell V, Constantino E, Ríos-Font R, Sodupe M, Rodríguez-Santiago L (2007) J Phys Chem A 111:9823–9829
43. Noguera M, Bertran J, Sodupe M (2008) J Phys Chem B 112:4817–4825
44. Cerda BA, Wesdemiotis C (1996) J Am Chem Soc 118:11884–11892
45. Basu S, Strobel SA (2001) Methods 23:264–275
46. Xing D, Tan X, Chen X, Bu Y (2008) J Phys Chem A 112:7418–7425
47. Oliva R, Cavallo L (2009) J Phys Chem B 113:15670–15678
48. Wu Y, Sa R, Li Q, Wei Y, Wu K (2009) Chem Phys Lett 467:387–392
49. Dinpajooh M, Keasler SJ, Truhlar DG, Siepmann JI (2011) Theor Chem Acc. doi:10.1007/s00214-011-0973-1
50. Jorgensen WL (2007) J Chem Theory Comput 3:1877
51. Lopes PEM, Roux B, MacKerell AD Jr (2009) Theor Chem Acc 124:11–28
52. Leverentz HR, Gao J, Truhlar DG (2011) Theor Chem Acc 129:3–13
53. Patel S, Brooks CL III (2004) J Comp Chem 25:1–16
54. Patel S, Mackerell AD, Brooks CL III (2004) J Comput Chem 25:1504–1514
55. Wang F, Jordan KD (2002) J Chem Phys 116:6973–6981
56. Lamoureux G, MacKerell AD, Roux B (2003) J Chem Phys 119:5185–5197
57. Lamoureux G, Harder E, Vorobyov IV, Roux B, MacKerell AD (2006) Chem Phys Lett 418:245–249
58. Yu H, Whitfield TW, Harder E, Lamoureux G, Vorobyov I, Anisimov VM, MacKerell AD, Roux B (2010) J Chem Theor Comput 6:774–786
59. Vorobyov IV, Anisimov VM, MacKerell AD (2005) J Phys Chem B 109:18988–18999
60. Vorobyov I, Anisimov VM, Greene S, Venable RM, Moser A, Pastor RW, MacKerell AD (2007) J Chem Theor Comput 3:1120–1133
61. Lopes PEM, Lamoureux G, Roux B, MacKerell AD (2007) J Phys Chem B 111:2873–2885
62. Lopes PEM, Lamoureux G, MacKerell AD (2009) J Comput Chem 30:1821–1838
63. Baker CM, Anisimov VM, MacKerell AD Jr (2011) J Phys Chem B 115:580–596
64. Chelli R, Schettino V, Procacci P (2005) J Chem Phys 122:234107
65. Chelli R, Procacci P (2002) J Chem Phys 117:9175–9199

66. Chillemi G, Coletta A, Mancini G, Sanna N, Desideri A (2010) Theor Chem Acc 127:293–302
67. Rode BM, Hofer TS, Randolf BR, Schwenk CF, Vchirawongkwin DX (2006) Theor Chem Acc 115:77–85
68. Lin H, Truhlar DG (2007) Theor Chem Acc 117:185–199
69. Yang ZZ, Wang CS (1997) J Phys Chem A 101:6315–6321
70. Wang CS, Yang ZZ (1999) J Chem Phys 110:6189–6197
71. Yang ZZ, Cui BQ (2007) J Chem Theory Comput 3:1561–1568
72. Yang ZZ, Wu Y, Zhao DX (2004) J Chem Phys 120:2541–2557
73. Wu Y, Yang ZZ (2004) J Phys Chem A 108:7563–7576
74. Zhao DX, Liu C, Wang FF, Yu CY, Gong LD, Liu SB, Yang ZZ (2010) J Chem Theory Comput 6:795–804
75. Wang FF, Zhao DX, Gong LD (2009) Theor Chem Acc 124:139–150
76. Yang ZZ, Li X (2005) J Phys Chem A 109:3517–3520
77. Li X, Yang ZZ (2005) J Chem Phys 122:084514
78. Zhang Q, Yang ZZ (2005) Chem Phys Lett 403:242–247
79. Yang ZZ, Zhang Q (2006) J Comput Chem 27:1–10
80. Boys SF, Bernardi F (1970) Mol Phys 19:553–566
81. Frisch MJ, Trucks GW, Schlegel HB, Scuseria GE, Robb MA, Cheeseman JR, J. A. Montgomery J, Vreven T, Kudin KN, Burant JC, Millam JM, Iyengar SS, Tomasi J, Barone V, Mennucci B, Cossi M, Scalmani G, Rega N, Petersson GA, Nakatsuji H, Hada M, Ehara M, Toyota K, Fukuda R, Hasegawa J, Ishida M, Nakajima T, Honda Y, Kitao O, Nakai H, Klene M, Li X, Knox JE, Hratchian HP, Cross JB, Adamo C, Jaramillo J, Gomperts R, Stratmann RE, Yazyev O, Austin AJ, Cammi R, Pomelli C, Ochterski JW, Ayala PY, Morokuma K, Voth GA, Salvador P, Dannenberg JJ, Zakrzewski VG, Dapprich S, Daniels AD, Strain MC, Farkas O, Malick DK, Rabuck AD, Raghavachari K, Foresman JB, Ortiz JV, Cui Q, Baboul AG, Clifford S, Cioslowski J, Stefanov BB, Liu G, Liashenko A, Piskorz P, Komaromi I, Martin RL, Fox DJ, Keith T, Al-Laham MA, Peng CY, Nanayakkara A, Challacombe M, Gill PMW, Johnson B, Chen W, Wong MW, Gonzalez C, Pople JA (2004) Gaussian 03. Revision D.01 edn. Gaussian, Inc., Wallingford, CT
82. Wintjens R, Liévin J, Rooman M, Buisine E (2000) J Mol Biol 302:395–410
83. Cornell WD, Cieplak P, Bayly CI, Gould IR, Merz KM, Ferguson DM, Spellmeyer DC, Fox T, Caldwell JW, Kollman PA (1995) J Am Chem Soc 117:5179–5197